RELATIVISTIC CODE APPLIED TO RADIATION GENERATION

A. T. Lin

Department of Physics
University of California, Los Angeles
Los Angeles, California, U. S. A.

ABSTRACT

In this chapter, a general algorithm for simulating a relativistic electromagnetic plasma is given. Emphasis is placed on how to handle the electron mass dependent on its energy and to treat boundary conditions for outgoing electromagnetic waves. The results of mode conversion from an extraordinary wave into an electrostatic Bernstein wave and radiation generation which exploits the relativistic effects of electrons such as gyrotron and auroral kilometric radiation are presented.

1. INTRODUCTION

The subject of this chapter is the interaction between charged particles and propagating electromagnetic waves. Of particular concern are the situations in which the relativistic effect of electron mass dependent on its energy plays influential roles in generating the electromagnetic wave and the wave amplitude is large such that nonlinear effects are important. Under these circumstances, the most effective tool in dealing with these phenomena is particle simulations.

In the early fifties electonic engineers[1] had already used particle simulations to investigate nonlinear state of various microwave devices. In their approaches, a steady state is assumed to exist. An electromagnetic wave with a specified frequency is injected into the interaction region and its spatial behaviour is followed. On the other hand, the nonlinear state in plasma physics is far more complicated. For instance, an electromagnetic wave can decay into other waves with different dispersive characteristics. A more general approach to particle simulation[2,3] was introduced in the late fifties

H. Matsumoto and T. Sato, Computer Simulation of Space Plasmas,

to study two-stream instability. Since that time a great deal of progress in computing power and simulation techniques has been made. Undoubtedly, particle simulations have made significant contribution to deeper understanding of plasma behavior.

In particle simulation the computer is employed to advance the motion of large number of charged partices, moving under the influence of the self-consistent and externally applied fields. The most general equations to represent these interactions are the Maxwell's equations

$$\begin{aligned} \frac{\partial \vec{E}}{\partial t} &= c\nabla \times \vec{B} - 4\pi \vec{J} \\ \frac{\partial \vec{B}}{\partial t} &= -c\nabla \times \vec{E} \\ \nabla \cdot \vec{B} &= 0 \\ \nabla \cdot \vec{E} &= 4\pi\rho \end{aligned} \tag{1}$$

and the relativistic equation of motion

$$\frac{d\vec{P}_j}{dt} = q_j \left\{ \vec{E} + \frac{\vec{P}_j \times \vec{B}}{m_j c \left(1 + \frac{P_j^2}{m_j^2 c^2} \right)^{1/2}} \right\} \tag{2}$$

where most of the symbols appearing in these equations have been defined in the previous chapters. Since computr time and storage are limited, discrete time step and spatial grids have to be used to change Eqs.(1) and (2) into finit difference equations. The basic schemes for solving these equations[4] have been described extensively in the previous chapters and will not be repeated. Here only the difference from the previous approach will be emphasized.

Instead of advancing the electromagnetic fields on each spatial grid[5], one can make use of Fast Fourier Transform (FFT) and advances their Fourier components[6]. To facilitate this we split $\vec{E}$ and $\vec{j}$ into transverse and longitudinal components; of course B only has transverse components. The longitudinal component of $\vec{E}$ is obtained as in the electrostatic case from Poisson's equaiton and the transverse $\vec{E}$ and $\vec{B}$ fields are obained by solving the Maxwell equations which now become

$$\begin{aligned} \frac{\partial \vec{E}_T(\vec{k},t)}{\partial t} &= i\vec{ck} \times \vec{B}_T(\vec{k},t) - 4\pi \vec{j}_T(\vec{k},t) \\ \frac{\partial \vec{B}_T(\vec{k},t)}{\partial t} &= -i\vec{ck} \times \vec{E}_T(\vec{k},t) \ , \end{aligned} \tag{3}$$

where the transverse components of the current are defined by

$$\vec{j}_T(\vec{k},t) = \vec{j}(\vec{k},t) - \frac{\vec{k}\vec{k} \cdot \vec{j}(\vec{k},t)}{k^2} \qquad (4)$$

Here again Eqs. (3) should be converted to finite difference equations in time and a leap frog scheme should be employed to solve for $\vec{E}_T$ and $\vec{B}_T$.

Since the Fourier transformation of a Gaussian distribution is again a Gaussian, the advantage of using a finite sized particle of Gaussian shape is easily included. Furthermore, as has been shown[6] that in contrast to the spatial finite differnce scheme, the phase velocity of electromagnetic wave is greater than c for all Fourier modes. This is also an important attribute of this algorithm. Especialy, if one is simulating a relativistic plasma as will be done here, and this is not the case, relativistic particles can exceed the light velocity in the spatial finit difference scheme. As consequence they emit spurious Cherenkov radiations which can easily swamp the pheneomenon we are interested in.

In treating the fully relativistic equations of motion for the charged particles, one now uses the particle momentum $\vec{P}j$ rather than the velocity $\vec{V}j$. However, in advancing $\vec{P}j$ as can be seen from Eq.(2), we need to know the average value of $\vec{P}j$ during a time step. Since $\vec{P}j$ also appears in the denominator of Eq.(2), it is very difficult to use the straightforward implicit scheme. Instead, one takes advantage of the fact that the magnetic force causes only a rotation of the particle about magnetic field but does not alter the particle energy. The scheme commonly adopted is the following, using only the electric field to advance $\vec{P}j$ by half time step, then use the updated $\vec{P}j$ to determine$|\vec{P}j|^2$. Equation (2) now resembles the nonrelativistic equations of motion and the usual implicit method can be used to advance $\vec{P}j$.

Various schemes of treating boundary conditions for outgoing electomagnetic waves will be discussed in Sec.2. The simulation results of radiation generation which exploit the relativistic effects of electrons will be presented in Sec 3 .

2. BOUNDARY CONDITIONS FOR OUTGOING ELECTROMAGNETIC WAVES

An electromagnetic wave originated in a plasma region can propagate into vacuum regions. If there are no reflicting walls to confine the radiation, the electomagnetic wave can reach infinity. In order to use a finite space to simulate an infinite region, some approximations have to be imposed on the Maxwell equaitons. There are three algorithms which have been successfully implemented in simulating various electomagnetic phenomena in plasma physics. They will be briefly described in this section. The first two algorithms are appropriate for the scheme which advances electromagnetic fields

on each spatial grid while the last algorithm is convenient for the scheme using FFT.

2.A. Decomposing Radiation Into Left-and Right-Going Waves

Assmue that space variations are in one direction (x) only and the electromagnetic wave is linearily polarized in y-direction. Let $F^{\pm}=E_y \pm B_z$. The electromagnetic components of Eq. (1) can be written as

$$\left(\frac{\partial}{\partial t} \pm c\frac{\partial}{\partial x}\right) F^{\pm} = \mp 4\pi J_y \tag{5}$$

In vacuum F^+ represents the wave traveling with velocity c in the negative x-direction wheareas F^- denotes the wave traveling with velocity c in the positive x-direction. Equation (5) can be solved by integrating separately the functions $F^{\pm}$ along the characteristic line of the light wave ($x \mp ct=$const.) which eliminates the spurious Chrenkov radiaitons. The grid spacing and time step are linked by the vacuum characteristics ($\Delta x/\Delta t=c$)[7]. The electromagnetic fields required for pushing particles can be determined from $E_y=(F^+ + F^-)/2$ and $B_z=(F^+ - F^-)/2$. The outgoing boundary condition for electromagnetic waves is simulated by assuming that the fictitious walls of the simulation system are radiation transparent.

The algorithm for more general cases involving variations in more than one direction is not quite so simple. Some attempts have been made without much success. A different algorithm which is commonly adopted in the field of laster fusion[8] will be discussed in the next sub-section.

2.B. Projection Operator

Consider a slab geometry which is periodic in the direction y but is finite in the direction x. In vacuum the wave equation for the electromagnetic field can be written as

$$\left(\frac{\partial}{\partial t} \pm c\cdot\hat{G}\frac{\partial}{\partial x}\right) A = 0 \tag{6}$$

where A is the wave vector potential and $\hat{G}$ is a projection operator which will be defined later. With properly chosen $\hat{G}$, Eq. (6) with the plus sign describes left-going waves (A_L) and with the minus sign represents right-going waves (A_R).

In order to demonstrate how the out-going waves can be absorbed by a properly chosen $\hat{G}$, consider a solution for Eq. (6) of the form

$$A = \left(A_R e^{ik_x x} + A_L e^{-ik_x x}\right) \exp[i(k_y y - \omega t)] \tag{7}$$

Substituting Eq. (7) into Eq. (6) gives

$$A_R + A_L = \frac{\hat{G}}{G_O} (A_R - A_L) \tag{8}$$

where

$$G_O = \frac{\omega}{ck_x} = (1 - \frac{c^2 k_y^2}{\omega^2})^{-1/2} \tag{9}$$

From Eq. (8) the reflection coefficient A_L/A_R is zero if $\hat{G}$ is chosen to be equal to Go. Empirically, Lindman[8] has found the best approximated expansion for $\hat{G}$ as follows

$$\hat{G} = 1 + \sum_{n=1}^{N} \hat{g}_n \tag{10}$$

where

$$\hat{g}_n = \frac{\alpha_n c^2 \hat{D}^2}{1 - \beta_n c^2 \hat{D}^2} \tag{11}$$

where the operator $\hat{D}=\partial_y/\partial_t$. Substitution of Eq.(11) into Eq.(6) and retaining only the plus sign yields

$$(\frac{\partial}{\partial t} + c\frac{\partial}{\partial x}) A = - c \sum_{n=1}^{N} \hat{h}_n \tag{12}$$

where $\hat{h}_n=\hat{g}_n \partial A/\partial x$. For each Fourier mode (ky), the usual finite difference scheme can be used to solve Eq. (12). Extra storage space which is small compared with the storage space for plasma region is required to implement this algorithm because it is only operative in the vacuum region. Lindman found that by choosing N=3, α=0.3269, 0.1272, 0.0309, and β=0.7375, 0.9838, 0.9966, the reflection coefficient is at its minimal value for a range of propagation angles from 0^O to 89^O.

2.C. Resistive boundary Layers

An electromagnetic wave propagates through a resisitive layer can be completely absorbed if the thickness of the layer is large enough. The property of a resistive layer can be modeled in particle code by adding an absorbing region on both sides of the plasma system to absorb the electromagnetic radiation leaving the plasma region. The schematic diagram of the simulation model is shown in Figure 1. The radiation field $\vec{E}_T(x,ky)$ is left unchanged between $x=0.5\ L_a$ and $x=0.5L_a+L_s$ but is multiplied by a function $f_a(x)$ which falls off from unity quadratically to zero in the absorbing region. Since the derivative of $f_a(x)$ is zero at x=0.5 La and (0.5 La+Ls), the reflection of an electromagnetic wave passing through these transition points is minimized. This algorithm can be easily implemented. However, it suffers the disadvantage of requiring more storage space to model the absorption regions than the previous two algorithms.

As an example, a mode conversion process[9] will be given to

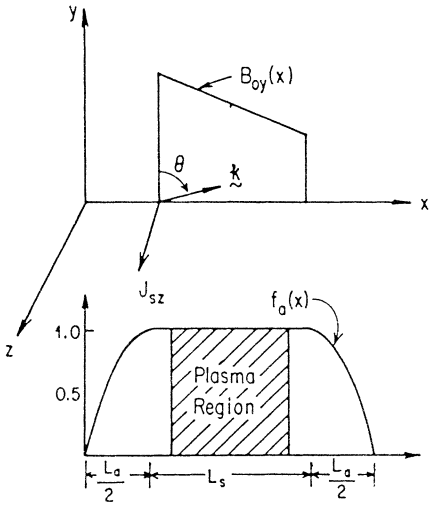

Figure 1. Schematic diagram of bounded simulation model. Radiation is absorbed by multiplying transverse electric field $E_T(x,ky)$ by the absorbing function $f_a(x)$ at each time step.

demonstrate the effectiveness of the outgoing wave boundary condition. For convenience, the resistive layer algorithm is chosen for our particle model. Consider an extraordinary wave of given ω_o propagates to the upper hybrid resonant layer, both its phase and group velocities approach zero in a collisionless cold plasma and the wave energy is converted into upper hybrid oscillations. For simplicity, consider a normal incident (Figure 1, $\theta=90^\circ$) extraordinary wave which is launched from the high field side into a plasma with uniform density. The magnetic field is assumed to vary linearly

$$\frac{B_o(x)}{B_o(0)} = 1 - \frac{x}{L_m} \tag{13}$$

where L_m is magnetic field scale length. The propagation of the extraordinary wave is governed by Maxwell's equations and the equation of motion which can be simplified to

$$\frac{d^2 E_z}{dx^2} + \frac{\omega_o^2}{c^2}\left\{1 - \frac{\omega_{pe}^2}{c^2}\frac{(\omega_o^2-\omega_{pe}^2+i\nu\omega_o)}{\omega_o^2-\omega_{pe}-\omega_{ce}^2+i\frac{\nu}{\omega_o}(2\omega_o^2-\omega_{pe}^2)}\right\} E_z = 0 \tag{14}$$

$$E_x = -i\, E_z \frac{\omega_{ce}}{\omega_o}\frac{\omega_{pe}^2}{\omega_o^2-\omega_{pe}^2-\omega_{ce}^2+i\frac{\nu}{\omega_o}(2\omega_o^2-\omega_{pe}^2)} \tag{15}$$

where ν is a phenomenological damping rate. In the computer

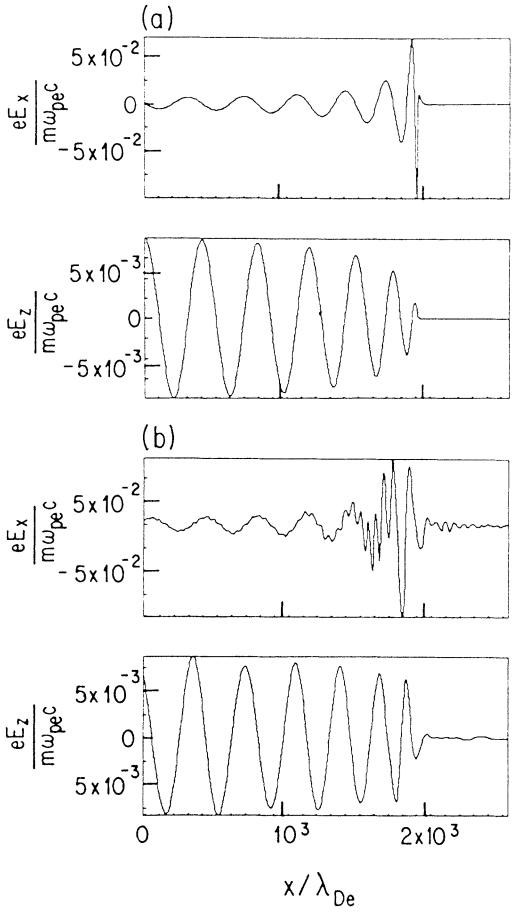

Figure 2. The electrostatic (E_x) and electromagnetic (E_z) field spatial distribution at ω_{pe}=500. (a) from cold plasma theory, (b) from computer simulation with immobile ions.

simulation, a current sheet is located at the high field side of the vacuum region. The current flows along the $\hat{z}$ direction and oscillates at a frequency ω_o to generate an extraordinary wave which when it reaches the plasma region will induce an electron to oscillate with a velocity $Vo=eE_o/m\omega_o$. The parameters for the simulation are chosen to be $Te/mc^2=1.7\times10^{-4}$, $Vo/c=0.01$, $\omega_o/\omega_{pe}=1.4$, $L_m/\lambda_{De}=6500$, $\omega_{ce}(0)/\omega_{pe}=1.53$

and the ions are immobile. Substituting this set of parameters into Eq.(14) and (15) and choosing $\nu/\omega_{pe}=4.5\times10^{-3}$ yield the spatial distribution of both the electromagnetic component (E_Z) and the electrostatic component (E_X). The theoretical result and the simulation result are displayed in fig.(2a) and Figure (2b) (at $\omega_{pe}t=500$) respectively. The agreements are quite good except that the simulation result shows that there is a short wavelength electrostatic Bernstein's wave which propagates out of the resonant region into the high field side with decreasing wavelength. This is a kinetic effect which the cold plasma theory is unable to reveal.

In the next section, the simulation results of two physical phenomena which rely on the relativistic effect of the electrons as their bunching mechanisms will be described.

3. ELECTRON CYCLOTRON MASER INSTABILITIES

The cyclotron radiation at the fundamental or at the first few harmonics of the cyclotron frequency by weakly relativistic electrons with non-equilibrium energy distribution and rotating in a magnetic field had been investigated by Twiss[10] in 1958. Based on his theory, in the past few years, a new class of high power and high efficiency microwave tubes[11] (Gyrotron) has emerged and the auroral kilometric radiation has been satisfactorily explained.

The basic energy transfer process in electron cyclotron maser instabilities can be visualized as follows: those electrons being accelerated by the wave gain energy and rotate slower whereas those electrons being decelerated by the wave lose energy and rotate faster; as a result of the electron inertia electrons bunch together azimuthally; if the initial mismatch $\Delta\omega=\omega_o-\omega_{ce}$ is greater than zero, the electron bunch is in the decelerating phase of the electromagnetic wave and a net transfer of enrgy from the electrons to the wave takes place.

3.A. Gyrotron Amplifiers

In order to simulate the performance of gyrotron amplifiers, what is called a stretched one and two halves dimensional code is used. The code is stretched in the sense that the transverse dependence of the electromagnetic field is assumed to be that of the fundamental empty waveguide mode and the transverse position of the electrons which have very small Larmor radius is fixed at the location where the maximum coupling between the electrons and fields takes place. Electrons are injected at the entrance to the interaction region and removed at the exit. An oscillating external current in front of the beam entrance models a matched RF input of arbitrary waveform. The resulting equaitons to be solvd in the circular waveguide configuration become

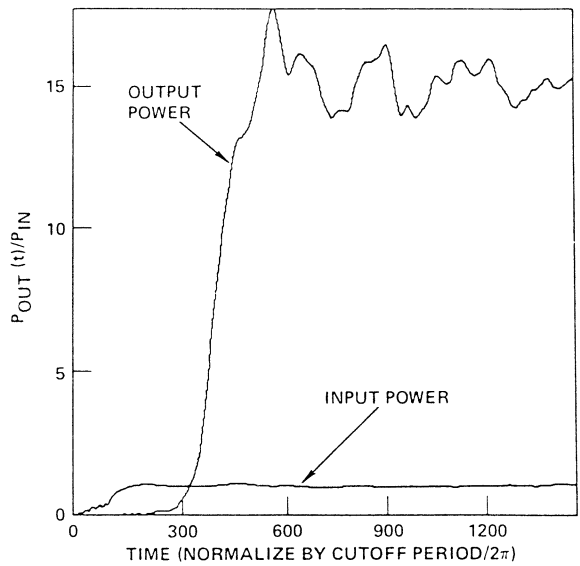

Figure 3. Output and input power monitored at the electron beam exit and entrance by calculating Poynting flux in time.

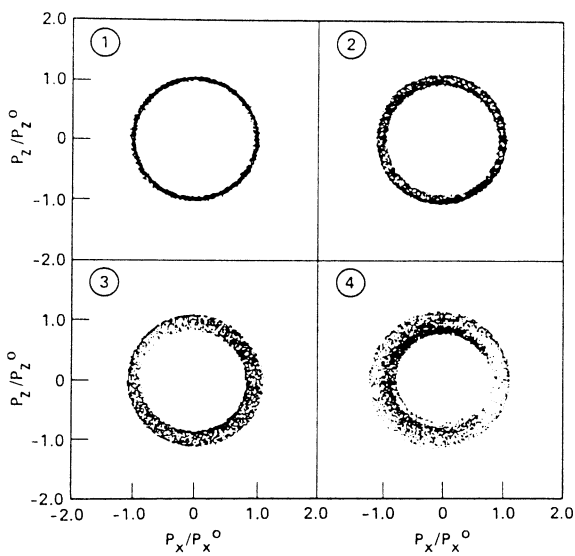

Figure 4. Electron positions in normalized transverse momentum space showing bunching at different axial beam locations going from beam entrance to beam exit in the order as labelled.

$$\frac{\partial B_r}{\partial t} = ick_x E_\phi$$
$$\frac{\partial B_x}{\partial t} = -\omega_{co} E_\phi \qquad (16)$$
$$\frac{\partial E_\phi}{\partial t} = ick_x B_r + \omega_{co} B_x - 4\pi J_\phi$$

where ω_{co} is the cut-off frequency of the waveguide. Outside the beam region the radiation is absorbed by using the resistive layer algorithm described in the previous section.

Simulation results for a 70 kev, $V_\perp/V_\parallel$=1.5, and 1 amp electron beam coupled to TE_{01} mode of a circular waveguide with radius Ro=0.535 cm and length Lo=10 cm under grazing condition will be discussed. A series of simulations was carried out. Figure 3 shows the time evolution of the input (500 watts) and output Poynting flux (power) which clearly indicates the desired amplification process. Figure 4 gives the spatial evolution (4 quarters along the beam) of the transverse momentum which illustrates that the electrons do give up their transverse energy along the interaction region and that phase trapping is the saturation mechanism. By changing the input power and frequency, a comparison of the nonlinear and liner bandwidth can be obtained (Figure 5). If bandwidth is defined as 3dB down, then the linear badwidth (80 watts input) is 4.5% versus a nonlinear bandwidth (500 watts input) of 7.5%.

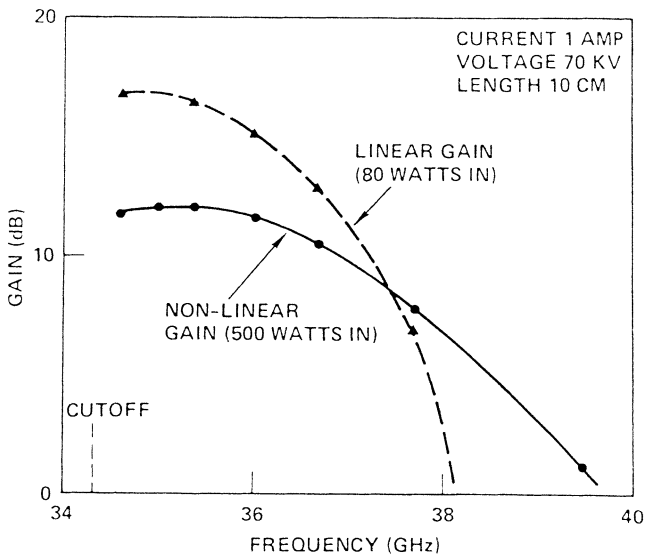

Figure 5. Linear and nonlinear gain versus frequency which determines the band width of an amplifier.

3.B. Auroral Kilometric Radiation

The electron cyclotron maser mechanism has recently been used to interpret the auroral kilometric radiation[12]. The theory predicts direct amplification of fast extraordinary mode radiation around the electron cyclotron frequency which agrees with the observed polarization and frequency of the radiation in the source region. The energy source for the instability comes from the anisotropic loss cone distribuiton of the electron energy which results from the reflection of enrgetic electrons (~1 kev) originated from the plasma-sheet region by the earth mirror magnetic fields.

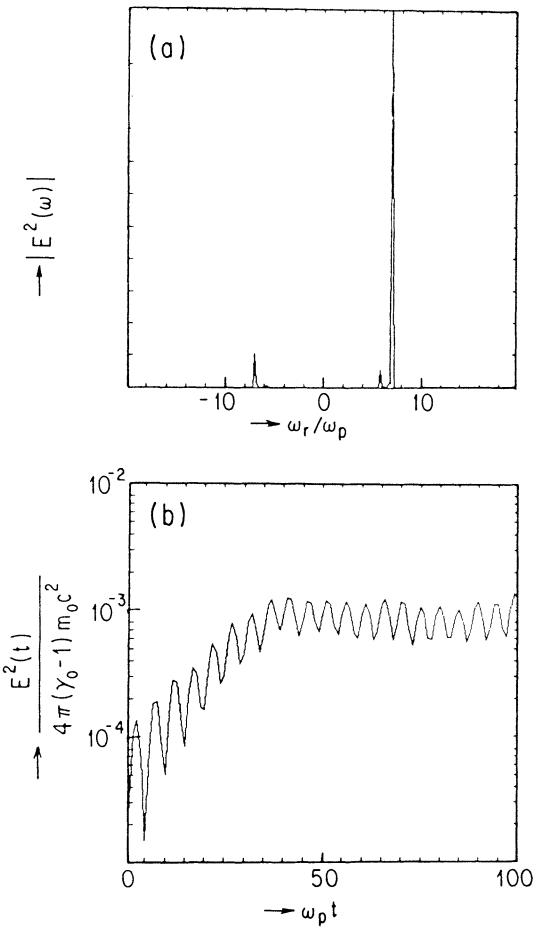

Figure 6. Simulations of electron cyclotron maser instability due to a loss cone distribution, (a) power spectrum, (b) time evolution, for the electronmagnetic field of the most unstable mode.

Most of the theoretical calculations are in the linear region. The only saturation mechanism which has been discussed is the quasi-linear flattening of the distribuiton function at the resonant region. A one and two-halves dimensional relativistic electromagnetic particle code with periodic boundary conditions is used to address the saturation mechanism of the electron cyclotron maser instability with parameters appropriate for the auroral region. The electron distribuiton function is taken to be

$$f_o(P_\perp^2, P_y) = AP_\perp^2 \exp\left(- \frac{P^2}{\Delta P^2} \right) \tag{17}$$

where A is a normalizaiton constant such that $\int d^3P f_o = 1$. $P_\perp$ and P_y are respectively the momentum of the electron perpendicular and parallel to the external magnetic field $B_o\hat{e}_y$. ΔP is a measure of the electron temperature

$$T_e = mc^2 \left\{ 1 + \frac{(\Delta P)^2}{m^2 c^2} \right\}^{1/2} - mc^2 \tag{18}$$

The electron distribution peaks at $P_\perp^2 = (\Delta p)^2$ which gives a population inversion in $P_\perp^2$. The following parameters are used: $\omega_{ce}/\omega_{pe} = 7.5$, $m^2c^2/(\Delta p)^2 = 50$, $\vec{K} \perp \vec{B}o$, and ions are immobile.

Figure 6a gives the power spectrum of the most unstable extraordinary mode which shows two peaks in the region of $\omega_r > 0$. From the cold plasma dispersion relation, there are two frequencies for each kx. The higher frequency mode corresponds to the fast wave ($v_p > c$) and the lower frequency mode corresponds to the slow wave ($v_p < c$). They are separated by the right-hand cutoff frequency. Initially, both modes are excited by the thermal noise. However, only the fast mode can be amplified by the electrons. Figure 6b displays the the time evolution of the most unstable mode which shows the desired exponential growth as well as the beat disturbance between the fast and slow waves. The growth rate determined from the simulation is $\omega_i/\omega_{ce} = 6.6 \times 10^{-3}$ which is very close to the theoretical prediction of 6.7×10^{-3}. The unstable mode is saturated at $\omega_{pe}t = 40$ and the conversion efficiency is about 1.5×10^{-3}.

At the time of saturation for the most unstable mode, the electron distribution function (Figure 7) still maintains a small positive slope. It is until $\omega_{pe}t = 70$ that the loss cone is completely filled by the electron energy diffusion due to the unstable waves. This agrees with the simulation result which shows that the total electromagnetic energy is saturated at $\omega_{pe}t = 70$ and reveals that it might not be correct to retain only the most unstable mode in evaluating the energy of the saturated radiation. The change in the electron distribution in time could render some initially stable modes unstable which would also contribute to the total saturated radiation energy.

Before comparing the simulation results with the observational results, a more realistic boundary condition which allows electrons to

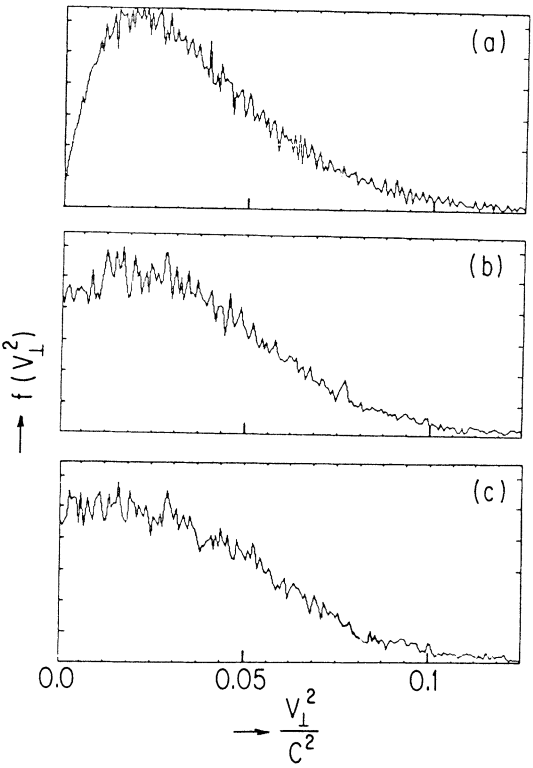

Figure 7. Time evolution of the electron energy distribution at (a) $\omega_{pe}t=0$, (b) $\omega_{pe}t=40$, (c) $\omega_{pe}t=70$.

go out if they are scattered into the loss cone should be implemented. A cold component of electrons originated from the ionosphere should also be included in the distribution function.

Ackowledgments

I wish to thank Mrs. Chih-Chien Lin for her valuable numerical support. This work has been supported by the National Science Foundation under Contract No. ECS81-15653 and PHY 80-26048.

REFERENCES

1. J. E. Rowe, Nonlinear Electron-Wave Interaction Phenomena (Academic Press), 1965.
2. O. Buneman, Phys. Rev., 115, 503, 1959.
3. J. M. Dawson, Phys. Fluids 5, 445, 1962.
4. J. M. Dawson and A. T. Lin, "Particle Simulation," Handbook of Plasma Physics, edited by A. Galeev and R. N. Sudan, North Holland Publishing Co., Amsterdam ,1983.
5. A. B. Langdon and B. F. Lasinski, Methods of Computational Physics, edited by J. Killen (Academic Press), 1976.
6. A. T. Lin, J. M. Dawson, and H. Okuda, Phys. Fluids, 17, 1995, 1974.
7. A. B. Langdon, Ph.D. Thesis, Princeton University, 1969.
8. E. L. Lindman, J. Comput. Phys., 18, 66, 1975.
9. A. T. Lin and Chih-Chien Lin, Phys. Rev. Lett. 47, 981, 1981.
10. R. Q. Twiss, Australian J. Phys., 11, 564, 1958.
11. M. Caplan, A. T. Lin, and K. R. Chu, International J. of Electronics, 53, 659, 1982.
12. C. S. Wu and L. C. Lee, Astrophys. J., 230, 621, 1979.